Laboratory Investigation (2018) 98:856–870
https://doi.org/10.1038/s41374-018-0051-6

ARTICLE

miR-9-5p, miR-124-3p, and miR-132-3p regulate BCL2L11 in tuberous sclerosis complex angiomyolipoma

Yi Cai[1,2] · Wenda Wang[1] · Hao Guo[1] · Hanzhong Li[1] · Yu Xiao[3] · Yushi Zhang[1]

Received: 20 September 2017 / Revised: 15 January 2018 / Accepted: 25 January 2018 / Published online: 14 March 2018

Abstract

Tuberous sclerosis complex (TSC) is a genetic disorder characterized by tumor formation in multiple organs, with over 80% of TSC patients developing angiomyolipomas (TSC-AMLs). However, the molecular events that contribute to TSC-AMLs are not well understood. Recent reports have demonstrated that microRNAs (miRNAs) are critical in TSC cortical tubers. However, little is known about the role of miRNAs in TSC-AMLs. In the current study, we analyzed changes in the miRNA and mRNA profiles in TSC-AMLs and matched normal adjacent tissues. A total of 15 differentially expressed miRNAs and 2664 mRNAs were identified. Using quantitative real-time PCR, we confirmed the results of the miRNA and mRNA profile experiments. Through bioinformatic analysis and luciferase reporter assays, we found that BCL2L11, an apoptotic activator, was the direct target of miR-9-5p, miR-124-3p, and miR-132-3p. Engineered expression of miR-9-5p, miR-124-3p, or miR-132-3p significantly regulated proliferation and apoptosis in $Tsc2^{-/-}$ cells. Manipulated expression of BCL2L11 also led to proliferation and apoptosis alterations in $Tsc2^{-/-}$ cells, in agreement with the effects of the above three miRNAs. In addition, BCL2L11 rescued the proliferation and apoptotic inhibition induced by miR-9-5p, miR-124-3p, and miR-132-3p in $Tsc2^{-/-}$ cells. This study provides supportive evidence that miR-9-5p, miR-124-3p, and miR-132-3p play a role in TSC-AMLs through the regulation of BCL2L11.

Introduction

Tuberous sclerosis complex (TSC) is an autosomal-dominant genetic disorder that results from a mutation in either the *TSC1* or *TSC2* gene [1]. The *TSC1* and *TSC2* gene products, hamartin and tuberin, respectively, form a protein complex that suppresses the mammalian target of the rapamycin (mTOR) pathway, which is a critical regulator of cell growth and proliferation [2, 3]. TSC is characterized by hamartomatous lesions in many organs, and up to 80% of patients with TSC develop renal angiomyolipomas (TSC-AMLs), which are composed of dysplastic blood vessels, smooth muscle-like cells, and adipose tissue [4]. Genetic analyses have shown that these different cell types within an individual AML are clonal, indicating that they must be derived from a neoplastic stem cell that has the capacity to differentiate into these different lineages [5, 6]. The latest evidence suggests that the neoplastic stem cell of renal AMLs should be renal epithelial cell [7]. The incidence of renal angiomyolipoma increases with age, and most patients develop multiple bilateral lesions that pose a significant tumor burden on the kidneys. Although they are mostly benign, TSC-AMLs can lead to a variety of complications, the most significant of which is rupture, causing renal hemorrhage and shock. Renin-dependent hypertension is also prevalent among TSC patients, and ~15% of TSC patients develop end-stage renal disease. TSC-AML is a leading cause of TSC-related death in adult patients [4].

These authors contributed equally: Yi Cai, Wenda Wang.

Electronic supplementary material The online version of this article (https://doi.org/10.1038/s41374-018-0051-6) contains supplementary material, which is available to authorized users.

✉ Yushi Zhang
zhangyushi2014@126.com

[1] Department of Urology, Peking Union Medical College Hospital, Chinese Academy of Medical Sciences and Peking Union Medical College, 100730 Beijing, China

[2] Department of Urology, Xiangya Hospital, Central South University, No.87 Xiangya Road, Changsha City 410008 Hunan Province, China

[3] Department of Pathology, Peking Union Medical College Hospital, Chinese Academy of Medical Sciences and Peking Union Medical College, 100730 Beijing, China

Therefore, fully elucidating the underlying mechanism of TSC-AML progression is critical and will be aided by a better understanding of its molecular genetic controls.

MicroRNAs (miRNAs) belong to a class of conserved endogenous non-coding small RNAs that post-transcriptionally regulate many genes and most cell processes [8]. Mature miRNAs are derived from pre-miRNA precursors composed of hundreds or thousands of nucleotides constituting monocistronic or polycistronic transcriptional units, and they anneal to complementary sites in the 3′ untranslated region (3′ UTR) of target transcripts, resulting in either transcript degradation or inhibition of protein translation [9]. A previous study provided supportive evidence that inflammation-related miRNAs specifically involved in the modulation of the interleukin (IL)-1R/Toll-like receptor (TLR) pathway play a role in TSC cortical tubers [10]. Dombkowski et al. [11] showed that a set of four miRNAs (miR-23a, miR-34a, miR-34b, and miR-532-5p) were coordinately overexpressed in epileptogenic tubers compared with adjacent non-tuber tissue and confirmed that the TSC1 3′ UTR was targeted by miR-23a and miR-34a. However, little is known about the involvement of miRNAs in TSC-AML, and no reports on their role in TSC-AML have been published to date.

The integration of mRNA and miRNA microarrays could provide a more comprehensive understanding of the regulatory mechanisms governing TSC-AML. We therefore analyzed the miRNA expression profiles together with gene expression profiles in TSC-AML tissue compared with matched normal adjacent tissues for the same populations. The integrated analysis of miRNA and mRNA expression data can help provide insight into the regulatory mechanisms governing TSC-AML.

Materials and methods

Patients and tissue specimens

This study protocol was approved by the Human Ethics Committee at Peking Union Medical College Hospital. The procedures for the collection and use of tissues were performed in accordance with the ethical standards set forth in the Declaration of Helsinki. Tissue was snap frozen in liquid nitrogen and stored at −80 ℃ until used for RNA isolation or protein extraction. Tumor tissues and matched normal adjacent tissues without hemorrhages or necrosis were selected by the same pathologist. Typical tissue for miRNA and mRNA array is shown in Figure S1. Multiple sections from the same tumor were combined to compensate for tumor heterogeneity. To identify the miRNA and mRNA signatures of TSC-AML, we determined the expression profiles of a cohort of four TSC-AML patients, designated the discovery set. A second cohort of six patients, designated the validation set, was recruited to validate the roles of specific miRNAs and mRNAs. Table S1 shows all of the patient demographics as well as the mutation types of the TSC patients. Figure S2 provides a flow chart outlining the bioinformatic analysis.

Cell culture and cell transfection

HEK-293T cells were obtained from the American Type Culture Collection. The $Tsc2^{-/-}$ MEF cell line, which has been described previously, was a gift from Hongbing Zhang (Chinese Academy of Medical Sciences and Peking Union Medical College, Beijing, People's Republic of China) [12, 13]. All cell lines were cultured in DMEM supplemented with 10% fetal bovine serum (FBS), 100 U/ml penicillin, and 100 mg/ml of streptomycin at 37 °C in a humidified 5% CO_2 atmosphere.

HEK-293T or $Tsc2^{-/-}$ MEF cells were seeded in 6-well plates, and transfection was conducted after 24 h. The BCL2L11-overexpressing lentivirus and the control lentivirus were purchased from GenePharma (Shanghai, China); 10^6 recombinant lentivirus-transducing units and 5 mg/ml polybrene (Sigma, USA) were added to each well with gentle mixing to infect the HEK-293T or $Tsc2^{-/-}$ MEF cells. Cell transfection with miR-24 mimics and inhibitors were conducted using Lipofectamine RNAiMAX (Invitrogen, USA) according to the manufacturer's instructions. For each well, equal doses (100 pmol) of miRNA mimics, inhibitors, siRNAs, or scrambled/negative control RNA were used. All RNA oligoribonucleotides were obtained from GenePharma (Shanghai, China).

Total RNA isolation (including miRNA)

Total RNA was isolated using TRIzol (Invitrogen, USA) and purified with an RNeasy mini kit (Qiagen, Germany) according to the manufacturer's instructions. RNA quality and quantity were assessed using a Nanodrop spectrophotometer (ND-1000, Nanodrop Technologies), and RNA integrity was determined by gel electrophoresis. All of the RNA samples were of good quality (260/280 nm absorbance ratios: 1.9~2.1). Each RNA sample was then divided into three aliquots, which were used for the miRNA microarray, the gene expression microarray, and real-time quantitative PCR.

miRNA and gene expression analysis

A miRCURY™ Hy3™/Hy5™ Power labeling kit (Exiqon, Denmark) was used for miRNA labeling according to the manufacturer's guidelines. Microarray analysis for miRNA profiling was conducted by Shanghai Kangcheng

Technology using the miRCURY^{TM} LNA Array system (v.18.0) according to the array manual (Exiqon, Denmark). Reverse transcription for first strand of cDNA was synthesized using an Invitrogen Superscript ds-cDNA synthesis kit (Invitrogen, USA). The ds-cDNA samples were labeled according to the manufacturer's instructions (Shanghai Kangcheng Technology, China). The Human 12 × 135K Gene Expression Array was manufactured by Roche NimbleGen. The miRNA and gene expression microarray raw data were normalized using quantile normalization and the robust multichip average (RMA) algorithm included in the NimbleScan software. The signal values were $\log_2$ transformed, and then the quantile and percentile shifts were applied to obtain equal distributions of the probe signal intensities. Comparative analysis between the samples from the TSC-AML and matched normal adjacent tissue groups was carried out using *t* tests (*p* values) and Benjamini–Hochberg false discovery rate (FDR) corrections (adjusted *p* values). The expression levels of genes and miRNAs were compared with those of the reference RNA and were determined to be differentially expressed if the adjusted *p* values were <0.05 and if the fold change (FC) was >2.0.

Real-time quantitative PCR analysis

Real-time quantitative PCR was performed using the miScript PCR System with 10× miScript Primer Assays for miRNAs (Qiagen, Germany) to confirm the array results. The U6 snRNA primer assay (Qiagen, Germany) was chosen as an endogenous reference for normalization, and all procedures were carried out according to the manufacturer's recommendations. To validate the different expression levels of the mRNAs determined by microarray, qPCR primers were selectively designed for 10 mRNAs that were found to be differentially expressed in the discovery screen; GAPDH was selected as the internal control. These primers are described in Table S2. Reverse transcription for first strand cDNAs was performed using an Invitrogen Superscript ds-cDNA synthesis kit (Invitrogen, USA). Melting curve analysis and agarose gel electrophoresis were used to assess the specificity of the qPCR products.

Gene ontology (GO) and kyoto encyclopedia of genes and genomes (KEGG) pathway analyses

GO and KEGG pathway analyses were performed using Cytoscape V2.8 (http://cytoscape.org/) with the ClueGO V1.3 plug-in. ClueGO determines the distribution of the target gene list across the GO terms and pathways. The *p* values were calculated using right-sided hypergeometric tests, and Benjamini–Hochberg adjustments were used for multiple test correction. An adjusted *p* value <0.05 indicated a statistically significant deviation from the expected distribution, and thus the corresponding GO terms and pathways were enriched in target genes. We analyzed all of the differentially expressed genes using GO and KEGG pathway analyses.

miRNA–mRNA enrichment and negative correlation analyses

Putative target gene sets of differentially expressed miRNAs were predicted using the following algorithms: miRBase (http://www.mirbase.org/), Miranda (http://www.microrna.org/), and TargetScan14 (http://www.targetscan.org/). The *p* values were calculated using right-sided hypergeometric tests, and Benjamini–Hochberg adjustments were used for multiple test correction. An adjusted *p* value <0.05 indicated a statistically significant deviation from the expected distribution. Pearson correlation coefficients between a particular miRNA and its predicted target mRNAs were computed using R (http://www.R-project.org) to determine whether the expression levels of each miRNA and of its mRNA targets were negatively correlated. The miRNA–mRNA interaction network was constructed using Cytoscape software.

Luciferase reporter assay

For dual luciferase assays, luciferase reporter pMIR-REPORT vectors (Promega, USA) containing the 3′ UTR of BCL2L11 with its wild-binding site (WT) or with mutant-binding sites (MUT) were specifically synthesized (GenePharma, China). HEK-293T cells were transfected with 10 ng of each pMIR-REPORT construct along with miRNA mimics/inhibitors or scrambled/negative controls and Lipofectamine 2000 reagent (Invitrogen, USA). After 48 h, the cells were lysed, and the firefly and Renilla luciferase activities were measured using the dual-luciferase reporter assay system (Promega, USA). Each fragment containing a putative miRNA-binding site was cloned into the pMIR-REPORT vector immediately downstream of the Renilla luciferase gene. The results are presented as the ratio of Renilla luciferase activity to firefly luciferase activity.

Western blot analysis

Frozen tissue was homogenized with a mortar and a pestle for each sample. Liquid nitrogen was added into the mortar during homogenization to keep the tissue frozen. Cold 1× cell lysis buffer with protease inhibitor cocktail was added to the frozen tissue powder, mixed and scooped into a 2 ml eppendorf tube. Then, the protein extract was centrifuged for 10 min at 14,000 × *g* in a cold centrifuge. Supernatant was transferred into a fresh 1.5 ml eppendorf tube and

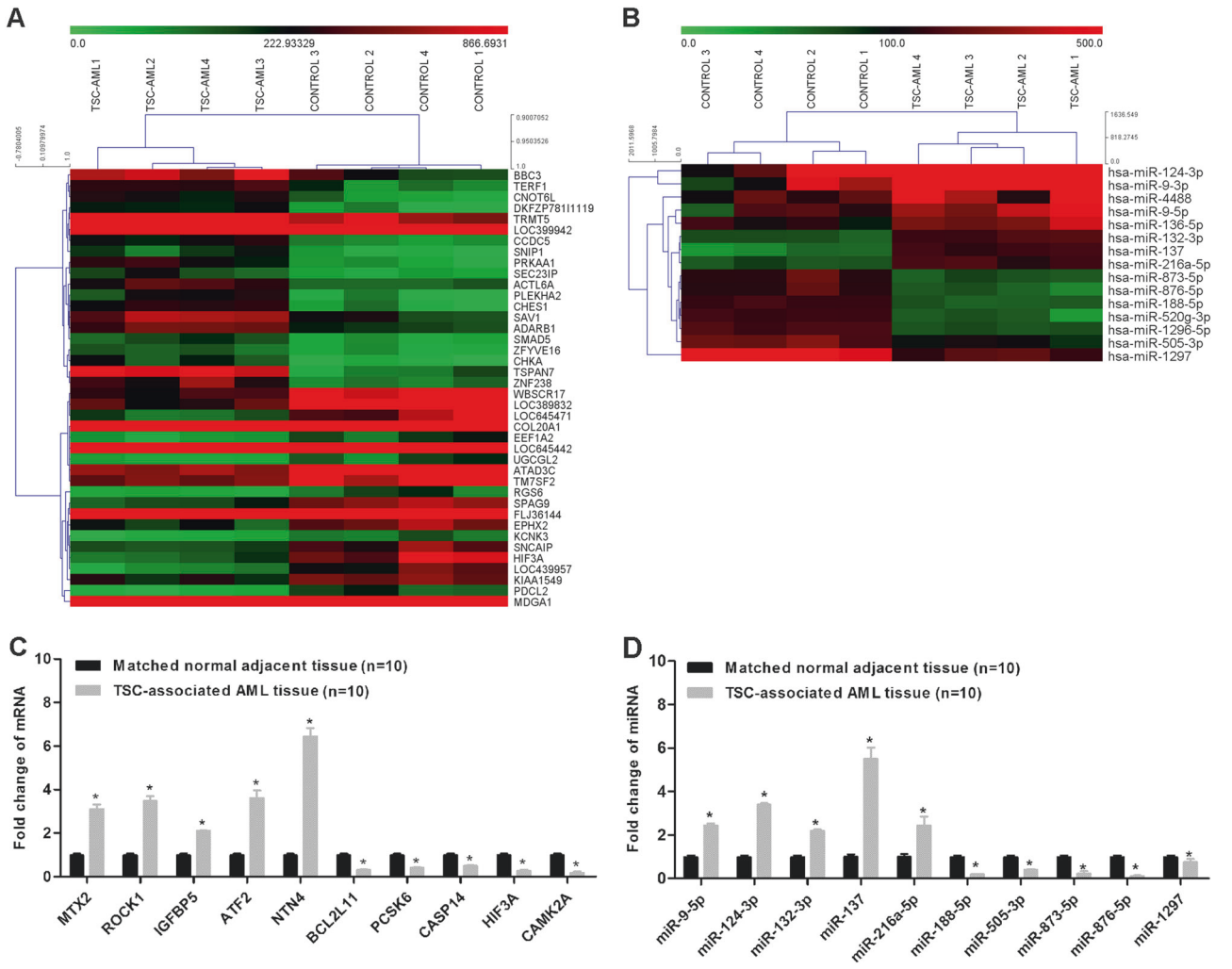

Fig. 1 Discovery and validation of differentially expressed genes and miRNAs. **a** Unsupervised hierarchical clustering according to the expression profiles of the top 40 most variable mRNAs between four TSC-AML tissues and matched normal adjacent tissues. **b** Unsupervised hierarchical clustering according to the expression profiles of the top 15 differentially expressed miRNAs between four TSC-AML tissues and matched normal adjacent tissues. **c** The miRNAs determined to be differentially expressed in all of the patients by microarray analysis were validated by qPCR. **d** The genes determined to be differentially expressed in all of the patients by microarray analysis were validated by qPCR. The column heights in the chart represent the average fold change in expression for each of the validated genes in the four TSC-AML tissues and matched normal adjacent tissues; the bars represent standard errors. $*p < 0.05$

smaller aliquots of each protein extract were stored at −80 °C. Total protein concentration was determined with the Bio-Rad Protein Assay Dye Reagent Concentrate (Bio-Rad, USA). Protein samples were separated on 10% SDS-PAGE gels, transferred to polyvinylidene fluoride (PVDF) membranes, and probed with goat polyclonal antibodies to BCL2L11 (Santa Cruz Biotechnology, USA) or GAPDH (Cell Signaling Technology, USA) overnight at 4 °C. After extensive washing, the membranes were incubated with secondary antibody conjugated to horseradish peroxidase (Cell Signaling Technology, USA) for 1 h at room temperature. Blots were developed using the enhanced chemiluminescence (ECL) system (PE Life Science, USA). The optical intensity of each stained protein band was determined using Quantity One software.

Cell proliferation analysis

Cell proliferation assays were conducted using a Cell Counting Kit-8 (CCK-8, Dojindo Laboratories, Japan) according to the manufacturer's instructions. The cells were seeded in 96-well plates at ~5000 cells per well and cultured in growth medium. Ten microliters of CCK-8 were added to 90 µl of culture medium at the indicated time. Subsequently, the cells were incubated at 37 °C for 2 h, and the optical density was measured at 450 nm.

Apoptosis analysis

Apoptosis was evaluated via annexin V and 7-AAD binding assays using a PE Annexin V Apoptosis Detection Kit I (BD

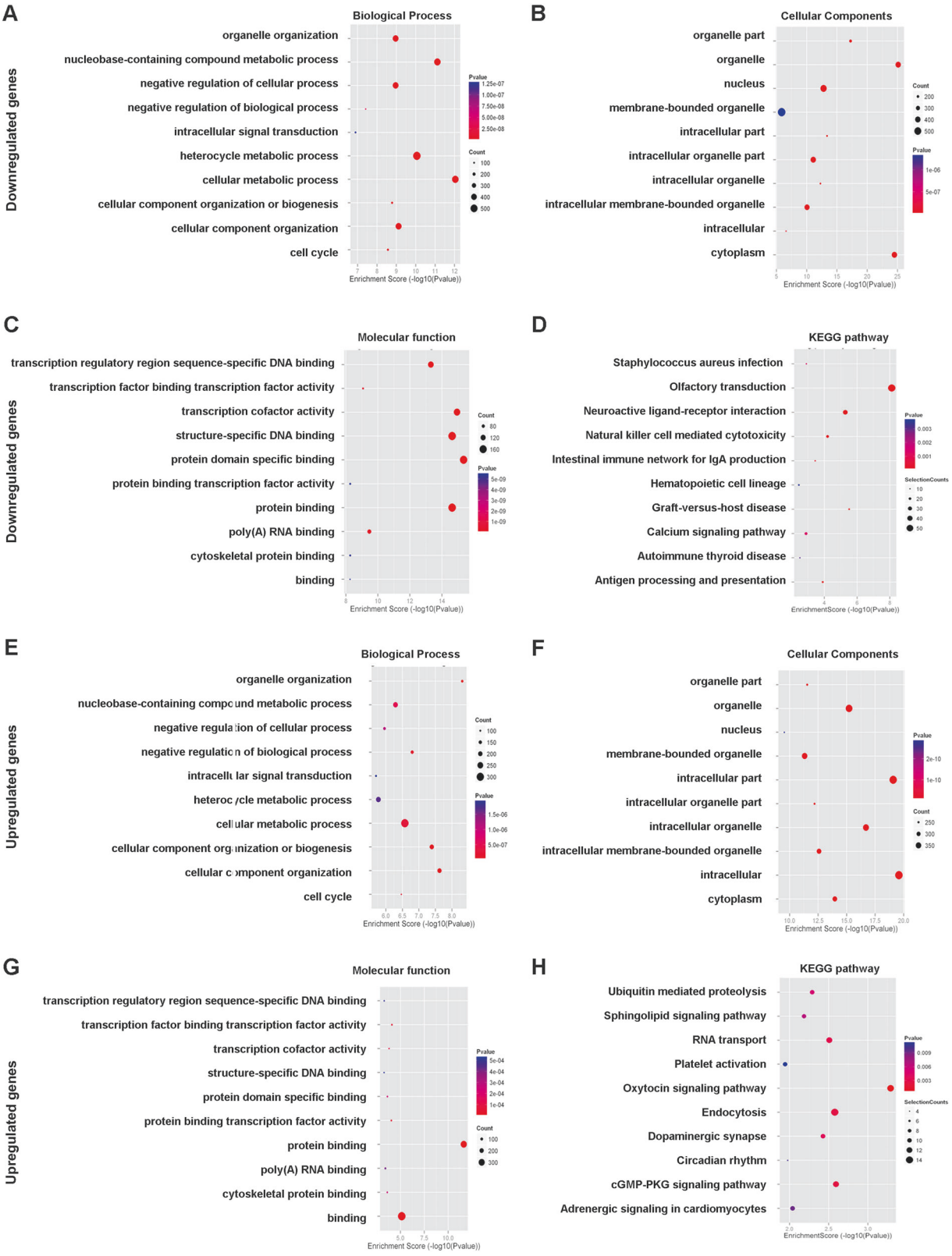
A
Biological Process
Downregulated genes
organelle organization
nucleobase-containing compound metabolic process
negative regulation of cellular process
negative regulation of biological process
intracellular signal transduction
heterocycle metabolic process
cellular metabolic process
cellular component organization or biogenesis
cellular component organization
cell cycle
Enrichment Score (-log10(Pvalue))
Pvalue
Count
B
Cellular Components
organelle part
organelle
nucleus
membrane-bounded organelle
intracellular part
intracellular organelle part
intracellular organelle
intracellular membrane-bounded organelle
intracellular
cytoplasm
Enrichment Score (-log10(Pvalue))
Count
Pvalue
C
Molecular function
Downregulated genes
transcription regulatory region sequence-specific DNA binding
transcription factor binding transcription factor activity
transcription cofactor activity
structure-specific DNA binding
protein domain specific binding
protein binding transcription factor activity
protein binding
poly(A) RNA binding
cytoskeletal protein binding
binding
Enrichment Score (-log10(Pvalue))
Count
Pvalue
D
KEGG pathway
Staphylococcus aureus infection
Olfactory transduction
Neuroactive ligand-receptor interaction
Natural killer cell mediated cytotoxicity
Intestinal immune network for IgA production
Hematopoietic cell lineage
Graft-versus-host disease
Calcium signaling pathway
Autoimmune thyroid disease
Antigen processing and presentation
EnrichmentScore (-log10(Pvalue))
Pvalue
SelectionCounts
E
Biological Process
Upregulated genes
organelle organization
nucleobase-containing compound metabolic process
negative regulation of cellular process
negative regulation of biological process
intracellular signal transduction
heterocycle metabolic process
cellular metabolic process
cellular component organization or biogenesis
cellular component organization
cell cycle
Enrichment Score (-log10(Pvalue))
Count
Pvalue
F
Cellular Components
organelle part
organelle
nucleus
membrane-bounded organelle
intracellular part
intracellular organelle part
intracellular organelle
intracellular membrane-bounded organelle
intracellular
cytoplasm
Enrichment Score (-log10(Pvalue))
Pvalue
Count
G
Molecular function
Upregulated genes
transcription regulatory region sequence-specific DNA binding
transcription factor binding transcription factor activity
transcription cofactor activity
structure-specific DNA binding
protein domain specific binding
protein binding transcription factor activity
protein binding
poly(A) RNA binding
cytoskeletal protein binding
binding
Enrichment Score (-log10(Pvalue))
Pvalue
Count
H
KEGG pathway
Ubiquitin mediated proteolysis
Sphingolipid signaling pathway
RNA transport
Platelet activation
Oxytocin signaling pathway
Endocytosis
Dopaminergic synapse
Circadian rhythm
cGMP-PKG signaling pathway
Adrenergic signaling in cardiomyocytes
EnrichmentScore (-log10(Pvalue))
Pvalue
SelectionCounts

◀ **Fig. 2** Top ten GO and KEGG pathways associated with the significantly dysregulated genes. **a** Ten top-ranked categories of GO biological processes associated with the downregulated gene list. **b** Ten top-ranked categories of GO cellular components associated with the downregulated gene list. **c** Ten top-ranked categories of GO molecular function associated with the downregulated gene list. **d** Ten top-ranked categories of KEGG pathways associated with the downregulated gene list. **e** Ten top-ranked categories of GO biological processes associated with the upregulated gene list. **f** Ten top-ranked categories of GO cellular components associated with the upregulated gene list. **g** Ten top-ranked categories of GO molecular function associated with the upregulated gene list. **h** Ten top-ranked categories of KEGG pathways associated with the upregulated gene list. The *p* values were calculated using hypergeometric tests and were corrected via Benjamini–Hochberg adjustments. The *p* values are expressed as negative logarithms (base 10)

Biosciences, USA) according to the manufacturer's instructions. At least 5×10^5 cells were analyzed for each sample. Control cells stained with annexin V-PE or 7-AAD alone were used as negative controls for the flow cytometry analysis.

Statistical analysis

All statistical analyses were performed with SPSS 19.0 software (SPSS, Chicago, IL, USA). Data are expressed as the mean ± standard deviation (M ± SD) from three separate experiments. Statistical significance was determined by paired or unpaired Student's *t* tests for the standardized expression data. $p < 0.05$ was considered statistically significant.

Results

Discovery and validation of differentially expressed genes and miRNAs

After applying a stringent filtering approach that compared TSC-AML samples with matched normal adjacent tissue (adjusted *p* value <0.05, fold change >2.0), we identified 691 upregulated and 1973 downregulated genes (Table S3) and 8 upregulated and 7 downregulated miRNAs (Table S4). Figure 1a shows a heat map of the expression profiles of the top 40 most variable mRNAs generated by cluster analysis. Figure 1b shows a heat map of 15 differentially expressed miRNAs generated by cluster analysis. These results indicate that gene expression in TSC-AMLs can be robustly different from that in matched normal adjacent tissue. Subsets of mRNAs (ten upregulated genes and ten downregulated genes) and miRNAs (five upregulated miRNAs and five downregulated miRNAs) that were identified to be differentially expressed by microarray analysis were selected for further validation in both the discovery set and the validation set. Comparison of the expression levels between the microarray data and the qPCR results demonstrated a strong correlation between the two platforms (Figs. 1c, d and S3). The fold changes in the expression levels of the tested mRNAs and miRNAs determined using qPCR were largely concordant with the microarray data.

GO and KEGG enrichment of differentially expressed genes

Four hundred fifty-four GO biological processes (*p* values <0.05) were associated with the downregulated genes. As shown in Fig. 2a, the top 10 significantly enriched biological processes were as follows: multicellular organismal process, single-multicellular organism process, response to stimulus, cell communication, signaling, single-organism signaling, G-protein-coupled receptor signaling pathway, cell–cell signaling, sensory perception of chemical stimulus, and sensory perception. Five hundred seventy-five GO biological processes (*p* values <0.05) were associated with the upregulated genes. As shown in Fig. 2e, the top 10 significantly enriched biological processes were as follows: organelle organization, cellular component organization, cellular component organization or biogenesis, negative regulation of biological process, cellular metabolic process, cell cycle, nucleobase-containing compound metabolic process, negative regulation of cellular process, heterocycle metabolic process, and intracellular signal transduction.

Eighty GO cellular components (*p* values <0.05) were associated with the downregulated genes. As shown in Fig. 2b, the top 10 significantly enriched cellular components were as follows: plasma membrane, cell periphery, plasma membrane part, intrinsic component of plasma membrane, membrane part, integral component of plasma membrane, intrinsic component of membrane, integral component of membrane, extracellular space and membrane. Sixty-five GO cellular components (*p* values <0.05) were associated with the upregulated genes. As shown in Fig. 2f, the top 10 significantly enriched cellular components were as follows: plasma membrane, cell periphery, plasma membrane part, intrinsic component of plasma membrane, membrane part, integral component of plasma membrane, intrinsic component of membrane, integral component of membrane, extracellular space and membrane.

One hundred and three GO molecular functions (*p* values <0.05) were associated with the downregulated genes. As shown in Fig. 2c, the top 10 significantly enriched molecular functions were as follows: receptor activity, signaling receptor activity, signal transducer activity, molecular transducer activity, transmembrane signaling receptor activity, G-protein-coupled receptor activity, substrate-specific channel activity, channel activity, passive transmembrane transporter activity, and cation channel activity. One hundred and two GO molecular functions (*p* values <0.05) were associated with the upregulated genes. As

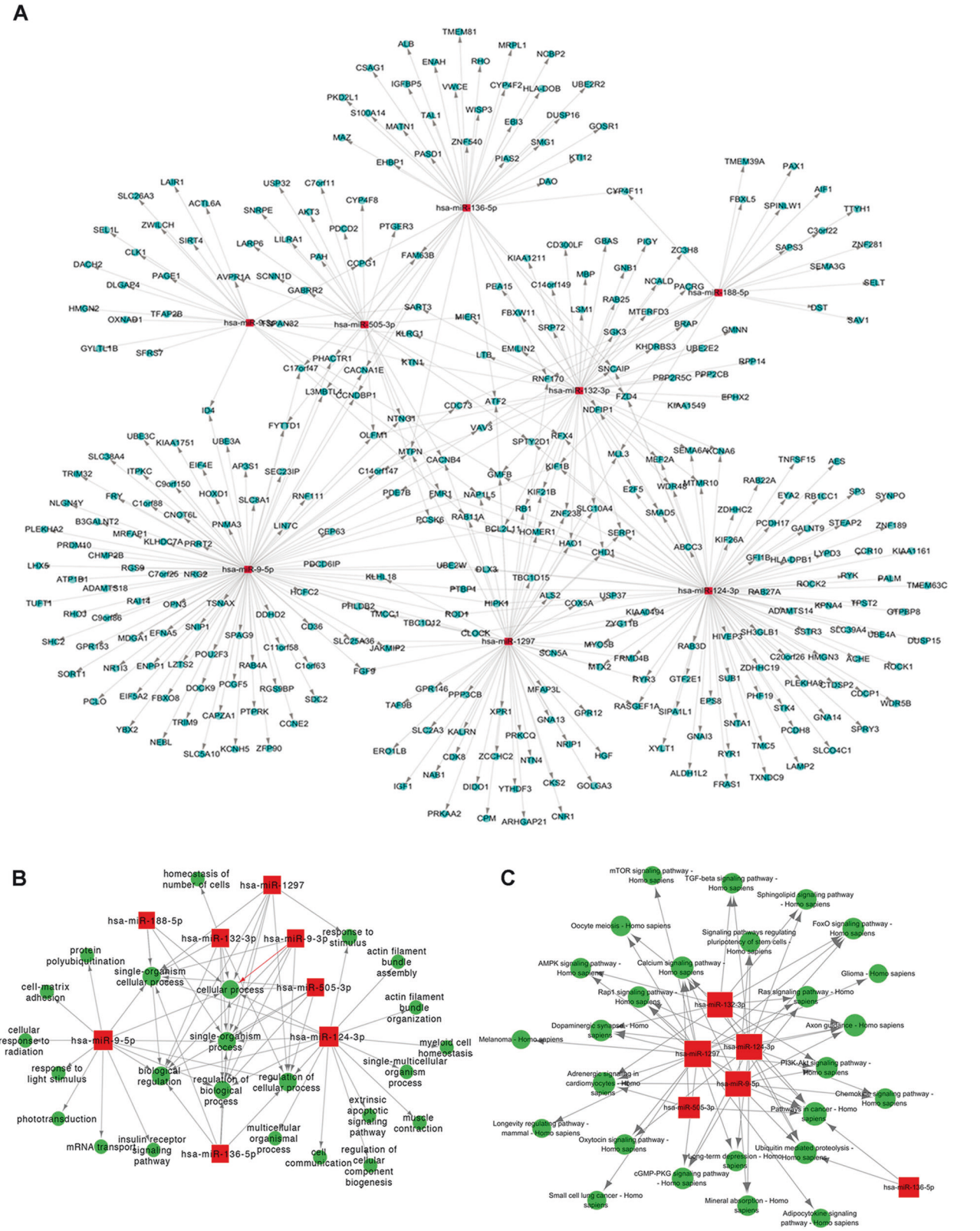

Fig. 3 The miRNA-target network, the involved GO biological processes, and the miRNA-regulated network. **a** Correlation network showing eight highly dysregulated miRNAs and their possible target mRNAs were constructed. **b** GO analysis of these target genes was performed. **c** KEGG pathway enrichment analysis showing a network of six highly enriched miRNA pathways

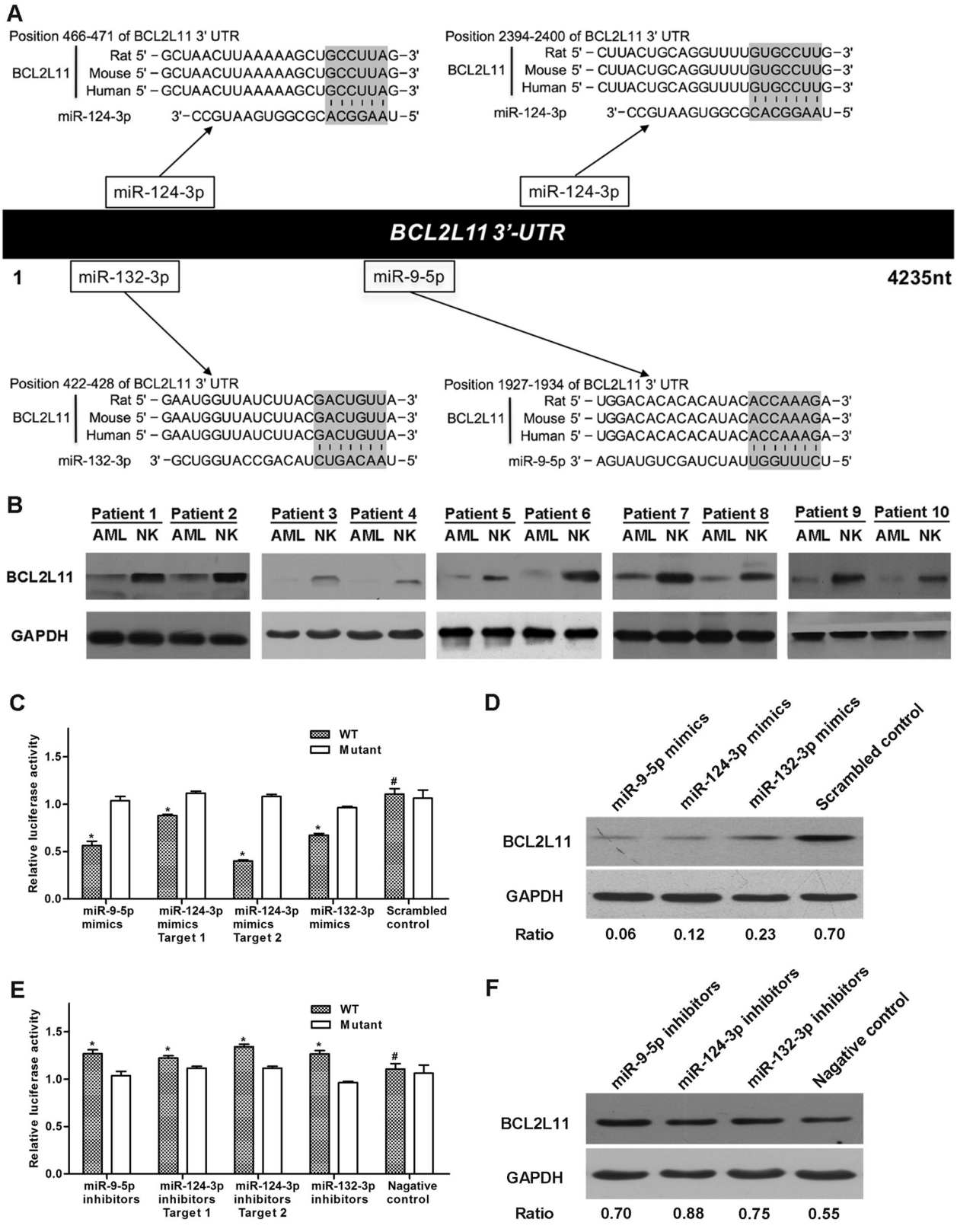

shown in Fig. 2g, the top 10 significantly enriched molecular functions were as follows: protein binding, binding, transcription factor binding transcription factor activity, protein binding transcription factor activity, transcription cofactor activity, protein domain-specific binding, cytoskeletal protein binding, poly(A) RNA binding, transcription

◀ **Fig. 4** Targeting of the BCL2L11 3′ UTR by miR-9-5p, miR-124-3p, and miR-132-3p. **a** Schematic representation of miRNA-binding sites within the BCL2L11 3′ UTR. **b** Western blot analysis of BCL2L11 expression in TSC-AML tissues and matched normal adjacent tissues ($n = 10$). **c** HEK-293T cells were co-transfected with firefly luciferase reporters containing either WT or mutant BCL2L11 3′ UTRs with miR-9-5p, miR-124-3p, or miR-132-3p mimics or the scrambled control. **d** Western blot analysis of BCL2L11 expression in $Tsc2^{-/-}$ cells transfected with miR-9-5p, miR-124-3p, or miR-132-3p mimics or the scrambled control. **e** HEK-293T cells were co-transfected with firefly luciferase reporters containing either WT or mutant BCL2L11 3′ UTRs with miR-9-5p, miR-124-3p, or miR-132-3p inhibitors or the negative control. **f** Western blot analysis of BCL2L11 expression in $Tsc2^{-/-}$ cells transfected with miR-9-5p, miR-124-3p, or miR-132-3p inhibitors or the negative control

regulatory region sequence-specific DNA binding, and structure-specific DNA binding.

Twenty-three KEGG pathways (p values <0.05) were associated with the downregulated genes. As shown in Fig. 2d, the top 10 significantly enriched biological processes were as follows: olfactory transduction, graft-versus-host disease, neuroactive ligand–receptor interaction, natural killer cell-mediated cytotoxicity, antigen processing and presentation, intestinal immune network for IgA production, Staphylococcus aureus infection, calcium signaling pathway, autoimmune thyroid disease, and hematopoietic cell lineage. Thirty-two KEGG pathways (p values <0.05) were associated with the upregulated genes. As shown in Fig. 2h, the top 10 significantly enriched pathways were as follows: oxytocin signaling pathway, cGMP-PKG signaling pathway, endocytosis, RNA transport, dopaminergic synapse, ubiquitin-mediated proteolysis, sphingolipid signaling pathway, adrenergic signaling in cardiomyocytes, circadian rhythm, and platelet activation.

Global miRNA-regulated network integration

To further explore the relationship between miRNA and TSC-AML progression, we utilized the online target gene prediction software programs miRBase, Miranda, and TargetScan to predict the target mRNAs of the identified miRNAs. The integrated analysis of miRNAs and mRNA expression levels is based on the assumption that increased or decreased expression of a specific miRNA results in, at least partially, decreased or increased expression of corresponding target mRNAs. Therefore, we investigated the existence of any inverse correlation between the up- or downregulated expression of an miRNA and its predicted targets (Figure S4), and a total of 5202 functional miRNA–mRNA pairs were connected by eight highly dysregulated miRNAs (Fig. 3a). Twenty-five GO biological processes (p values <0.05) were associated with these dysregulated mRNAs. As shown in Fig. 3b, the top six significantly enriched biological processes were as follows: single-organism signaling, cellular process, regulation of cellular process, biological regulation, regulation of biological process, and single-organism cellular process. Twenty-six KEGG pathways (p values <0.05) were associated with the dysregulated genes. As shown in Fig. 3c, KEGG pathway enrichment analysis showed a network of six highly enriched miRNA pathways. The top ten significantly enriched pathways included the PI3K-Akt signaling pathway, pathways in cancer, Ras signaling pathway, calcium signaling pathway, Rap1 signaling pathway, dopaminergic synapse, adrenergic signaling in cardiomyocytes, oxytocin signaling pathway, cGMP-PKG signaling pathway, and ubiquitin-mediated proteolysis.

Targeting of the BCL2L11 3′ UTR by miR-9-5p, miR-124-3p, and miR-132-3p

Each miRNA has many target mRNAs; a single mRNA can also be regulated by more than one miRNA. BCL2L11, an apoptotic activator, stood out as an attractive candidate, and its 3′ UTR contains putative recognition sites that could bind to miR-9-5p, miR-124-3p, and miR-132-3p, indicating the possible role of these three miRNAs in modulating BCL2L11 (Fig. 4a). The expression of the BCL2L11 protein was clearly decreased in TSC-AML tissues compared with matched normal adjacent tissue, suggesting that BCL2L11 expression may be involved in the progression of TSC-AML (Fig. 4b). To verify whether BCL2L11 is the target of miR-9-5p, miR-124-3p, and miR-132-3p, we constructed 3′ UTR luciferase reporters with WT BCL2L11 containing each of the potential three miRNA recognition elements individually as well as corresponding 3′ UTR mutants. A construct with Renilla luciferase only acted as a control. The results showed that HEK-293T cells co-transfected with miR-9-5p, miR-124-3p, and miR-132-3p mimics or inhibitors with the WT BCL2L11 reporter displayed decreased or increased luciferase activities, respectively, compared with the control groups, whereas the luciferase activity of the mutant BCL2L11 reporter significantly changed (Fig. 4c, e). Furthermore, western blotting showed that miR-9-5p, miR-124-3p, and miR-132-3p mimics downregulated the expression of miR-9-5p, miR-124-3p, and miR-132-3p, while miR-9-5p, miR-124-3p, and miR-132-3p inhibitors upregulated the expression of miR-9-5p, miR-124-3p, and miR-132-3p (Fig. 4d, f). These results indicated that miR-9-5p, miR-124-3p, and miR-132-3p can directly regulate BCL2L11.

miR-9-5p, miR-124-3p, and miR-132-3p regulate cell proliferation and apoptosis in $Tsc2^{-/-}$ cells

To explore whether and how miR-9-5p, miR-124-3p, and miR-132-3p regulate cell proliferation and apoptosis in

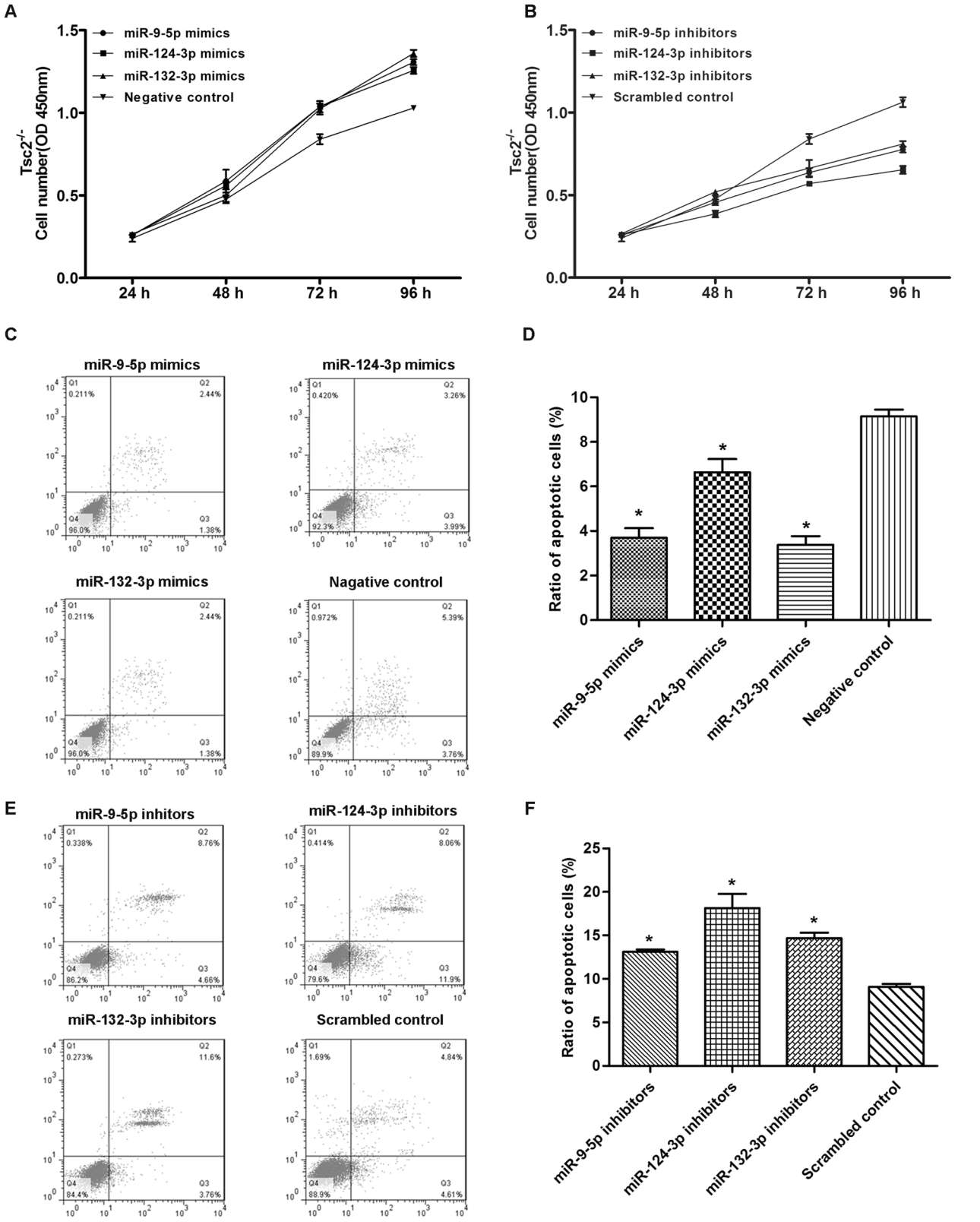

$Tsc2^{-/-}$ cells, we overexpressed these three miRNAs in $Tsc2^{-/-}$ cells. CCK-8 assays showed that $Tsc2^{-/-}$ cells transfected with miR-9-5p, miR-124-3p, or miR-132-3p mimics showed increased cell proliferation (Fig. 5a). In addition, the overexpression of miR-9-5p, miR-124-3p, or miR-132-3p markedly decreased the percentage of

◀ **Fig. 5** The role of miR-9-5p, miR-124-3p, and miR-132-3p in the regulation of proliferation and apoptosis in Tsc2$^{-/-}$ cells. **a** CCK-8 assays were performed 24, 48, 72, and 96 h after the transfection of Tsc2$^{-/-}$ cells with miR-9-5p, miR-124-3p, or miR-132-3p mimics or the scrambled control. **b** CCK-8 assays were performed 24, 48, 72, and 96 h after the transfection of Tsc2$^{-/-}$ cells with miR-9-5p, miR-124-3p, or miR-132-3p inhibitors or the negative control. **c**, **d** Tsc2$^{-/-}$ cells were transfected with equal doses of miR-9-5p, miR-124-3p, or miR-132-3p mimics or the scrambled control. The cell apoptosis profiles were analyzed by flow cytometry. The bi-parametric histogram shows cells in early (bottom right quadrant) and late (top right quadrant) apoptotic states. Viable cells are double negative (bottom left quadrant). **c** Representative image. **d** Quantitative analysis. **e**, **f** Tsc2$^{-/-}$ cells were transfected with equal doses of miR-9-5p, miR-124-3p, or miR-132-3p inhibitors or the negative control. The cell apoptosis profiles were analyzed by flow cytometry. The bi-parametric histogram shows cells in early (bottom right quadrant) and late (top right quadrant) apoptotic states. Viable cells are double negative (bottom left quadrant). **e** Representative image. **f** Quantitative analysis

apoptotic cells when compared with cells transfected using the negative control (Fig. 5c, d). Conversely, knockdown of miR-9-5p, miR-124-3p, or miR-132-3p inhibited cell proliferation (Fig. 5b). Moreover, downregulation of miR-9-5p, miR-124-3p, or miR-132-3p markedly increased the percentage of apoptotic cells when compared with cells transfected using the scrambled control (Fig. 5e, f). Taken together, these results indicate that miR-9-5p, miR-124-3p, and miR-132-3p are involved in the regulation of cell proliferation and apoptosis in Tsc2$^{-/-}$ cells.

BCL2L11 regulates cell proliferation and apoptosis in Tsc2$^{-/-}$ cells

Subsequently, we investigated whether overexpression or knockdown of BCL2L11 impacts cell proliferation and apoptosis in Tsc2$^{-/-}$ cells. Efficient knockdown and overexpression of BCL2L11 in Tsc2$^{-/-}$ cells are shown in Fig. 6a–c. Tsc2$^{-/-}$ cells transfected with BCL2L11 siRNA showed increased cell proliferation; in contrast, transfection with a lentivirus overexpressing BCL2L11 had the opposite effect on cell proliferation (Fig. 6d). In addition, transfecting Tsc2$^{-/-}$ cells with BCL2L11 siRNA markedly decreased the percentage of apoptotic cells when compared with cells transfected using control siRNA, whereas transfecting Tsc2$^{-/-}$ cells with a lentivirus overexpressing BCL2L11 increased cell apoptosis (Fig. 6e, f). Taken together, our results suggest that BCL2L11 is crucial for the proliferation and apoptosis of Tsc2$^{-/-}$ cells.

BCL2L11 rescues the effects of miR-9-5p, miR-124-3p, and miR-132-3p related to the regulation of proliferation and apoptosis in Tsc2$^{-/-}$ cells

To provide further evidence that miR-9-5p, miR-124-3p, and miR-132-3p are involved in the regulation of proliferation and apoptosis in TSC-AML, we used lentivirus particles and miR-9-5p, miR-124-3p, or miR-132-3p mimics to overexpress BCL2L11 in Tsc2$^{-/-}$ cells simultaneously. As shown in Fig. 7a, b, co-transfection of miR-9-5p, miR-124-3p, or miR-132-3p mimics and BCL2L11 lentivirus particles rescued BCL2L11 expression compared with single transfections of miR-9-5p, miR-124-3p, or miR-132-3p mimics (Fig. 4d). Moreover, overexpression of BCL2L11 in Tsc2$^{-/-}$ cells rescued the cellular proliferation (Fig. 7c) and apoptosis inhibition (Fig. 7d) induced by these three miRNAs compared with the single transfection of miR-9-5p, miR-124-3p, or miR-132-3p mimics (Fig. 4a, c). Taken together, our results suggest that miR-9-5p, miR-124-3p, or miR-132-3p might promote proliferation and inhibit apoptosis in Tsc2$^{-/-}$ cells by silencing BCL2L11.

Discussion

Through microarray profiling, we identified 15 miRNAs and 2664 mRNAs that were differentially expressed in TSC-AML tissues compared to matched normal adjacent tissues. We selected and confirmed the expression of a number of these miRNAs and mRNAs using real-time PCR in samples from both the discovery and validation groups. The expression of these miRNAs and the global profiles of the mRNAs was integrated, and the findings showed that the *BCL2L11* gene identified in our mRNA microarray data showed a high level of association with miR-9-5p, miR-124-3p, and miR-132-3p, which might contribute to TSC-AML by promoting proliferation and inhibiting apoptosis. We used a luciferase reporter assay to demonstrate targeting of the BCL2L11 3′ UTR by miR-9-5p, miR-124-3p, and miR-132-3p. Engineered expression of miR-9-5p, miR-124-3p, or miR-132-3p significantly regulated proliferation and apoptosis in Tsc2$^{-/-}$ cells. Manipulated expression of BCL2L11 in Tsc2$^{-/-}$ cells also led to alterations in proliferation and apoptosis, in agreement with the effects of above three miRNAs. In addition, BCL2L11 rescued the cell proliferation and apoptosis inhibition promoted by miR-9-5p, miR-124-3p, and miR-132-3p in Tsc2$^{-/-}$ cells. These studies reveal the importance of BCL2L11 targeting by miR-9-5p, miR-124-3p, and miR-132-3p as a novel regulatory network in TSC-AML.

BCL2L11 is a member of the BCL-2 family that is located in the outer membrane of mitochondria, where it acts as an important regulator, mediating excitotoxic apoptosis, apoptosis-inducing factor translocation, and mitochondrial depolarization [14, 15]. BCL2L11 has been shown to be critical for apoptosis in B and T lymphocytes, macrophages, and granulocytes [16]. In addition to neutralizing anti-apoptotic proteins, BCL2L11 promotes apoptosis by binding to Bax, which causes a conformational

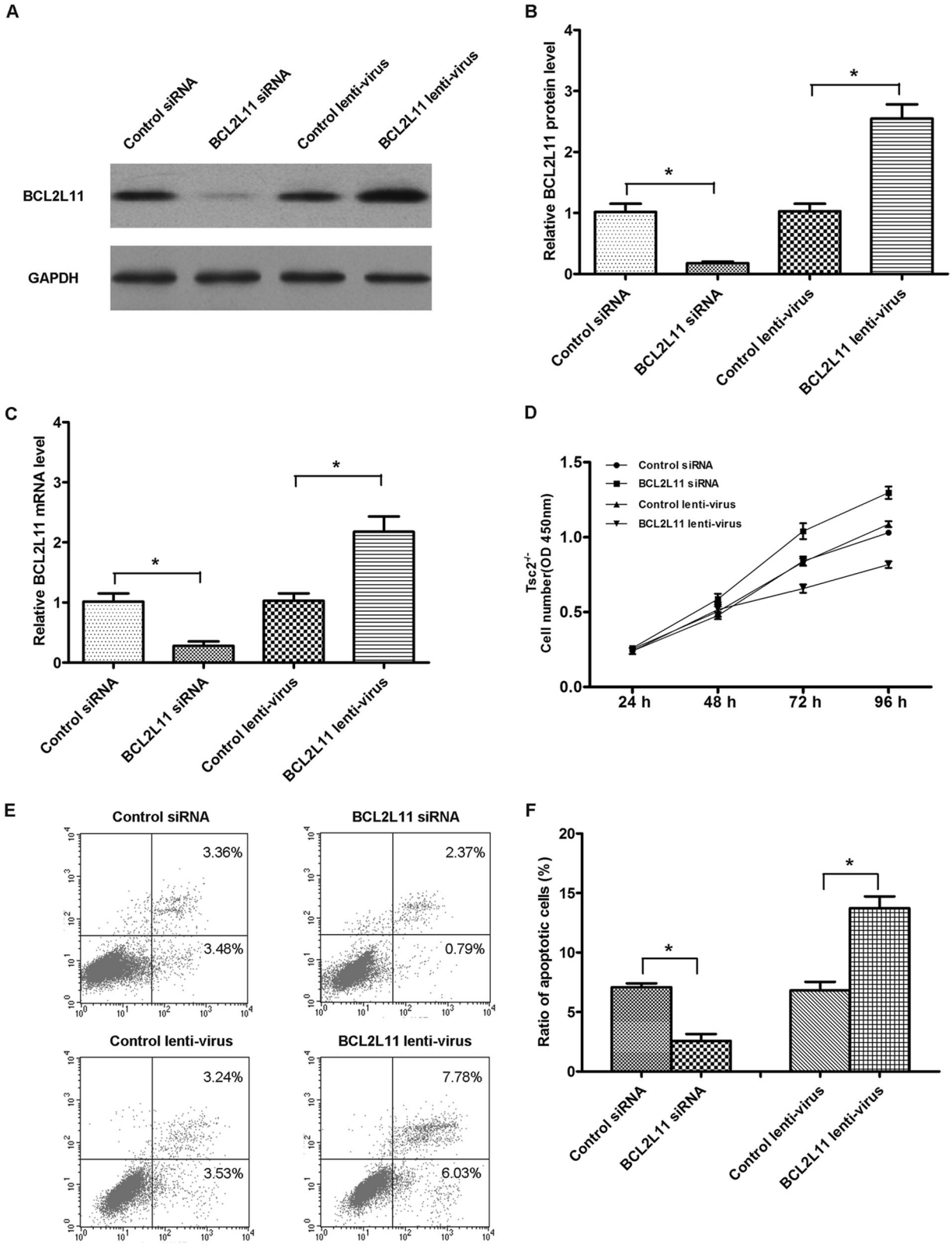

change in Bax that leads to its activation [17]. The anti-apoptotic BCL2 members have multiple domains, while the pro-apoptotic members of the BCL2 family, including BCL2L11, are BH3-domain-only proteins [18, 19]. While the role of BCL2L11 in these biological processes has been reported, its role in TSC-AML remains unknown,

◀ **Fig. 6** Downregulation of BCL2L11 by siRNA and upregulation of BCL2L11 via an overexpression lentivirus in $Tsc2^{-/-}$ cells. **a**, **b** Western blotting analysis of BCL2L11 protein levels in $Tsc2^{-/-}$ cells treated with control siRNA, BCL2L11 siRNA, control lentivirus, or BCL2L11 lentivirus. **a** Representative image. **b** Quantitative analysis. **c** Real-time quantitative PCR analysis of BCL2L11 mRNA levels in $Tsc2^{-/-}$ cells treated with control siRNA, BCL2L11 siRNA, control lentivirus, or BCL2L11 lentivirus. **d** CCK-8 assays were performed 24, 48, 72, and 96 h after the transfection of $Tsc2^{-/-}$ cells with control siRNA, BCL2L11 siRNA, control lentivirus, or BCL2L11 lentivirus. **e**, **f** $Tsc2^{-/-}$ cells were transfected with equal doses of control siRNA, BCL2L11 siRNA, control lentivirus, or BCL2L11 lentivirus. Cell apoptosis profiles were analyzed by flow cytometry. The bi-parametric histogram shows cells in early (bottom right quadrant) and late (top right quadrant) apoptotic states. Viable cells are double negative (bottom left quadrant). **e** Representative image. **f** Quantitative analysis

emphasizing the urgent need to fully elucidate the mechanisms that govern BCL2L11 regulation.

MiRNAs have emerged as mediators of gene expression [20]. They direct the regulation of cellular processes including differentiation, proliferation, cell–cell interaction, cell death, metabolism, and many diseases. Previous studies have provided supportive evidence that miRNAs play a role in TSC cortical tubers [10, 11]; however, the role of miRNAs in the kidneys of TSC patients has not previously been investigated. Another important aim of this study was to determine the possible regulatory role of miRNAs in TSC-AML. Several potential-binding sites were observed in the 2664 dysregulated genes and 15 dysregulated miRNAs in TSC-AML tissues identified by bioinformatic prediction. miR-9-5p, miR-124-3p, and miR-132-3p were predicted to target the 3′ UTR of BCL2L11 in the miRNA–mRNA network. miR-9-5p is broadly conserved in animals and was first identified as a crucial regulator for the development and maturation of the nervous system as well as in tumors outside the nervous system [21, 22]. A previous study demonstrated that miR-9-5p could specifically regulate the translation of BCL2L11 and induce increased expression of BCL2L11 in ischemic stroke, which then leads to neuronal apoptosis [23]. miR-124-3p is the most abundant miRNA in the brain, and it is involved in stem cell regulation and neurodevelopment [24, 25]. miR-132-3p has been shown to play an important role in synaptic transmission, inflammation, angiogenesis, and even cancer [26–28]. In endothelial cells, angiogenic factors, such as VEGF and bFGF, can promote the transcription of miR-132-3p, which further silences p120RasGAP expression and prevents its active conformation to induce proliferation [26]. In this study, we found that overexpressing miR-9-5p, miR-124-3p, and miR-132-3p promoted proliferation and inhibited apoptosis in $Tsc2^{-/-}$ cells and that BCL2L11 reduction mimicked miR-9-5p, miR-124-3p, and miR-132-3p induction. Interestingly, we observed that the restoration of BCL2L11 expression successfully attenuated the pro-proliferative and anti-apoptotic effects of miR-9-5p, miR-124-3p, and miR-132-3p on $Tsc2^{-/-}$ cells. These results suggest that the targeting of BCL2L11 is a major mechanism by which miR-9-5p, miR-124-3p, and miR-132-3p exert their tumor-promoting functions. Therefore, the modulation of BCL2L11 by miR-9-5p, miR-124-3p, and miR-132-3p might at least partially explain why the upregulation of these miRNAs in TSC-AML can promote cell proliferation and inhibit cell apoptosis in $Tsc2^{-/-}$ cells.

To investigate how these signature miRNAs really participate in the gene alteration of TSC-AML in depth, we performed bioinformatic analyses. GO analysis is widely recognized as a leading tool for the organization and functional annotation of molecular attributes [29]. For greater insight into the data, we also performed signal pathway analysis using the KEGG pathway mapping tool, which is based on gene ontology classifications. The GO and KEGG pathway analyses of the commonly dysregulated genes also provided us with substantial information about the development and progression of TSC-AML. The GO analysis revealed that single-organism signaling, cellular process, regulation of cellular process, biological regulation, regulation of biological process, and single-organism cellular process were among the most prominent biological processes, while PI3K-Akt signaling pathway, pathways in cancer, Ras signaling pathway, calcium signaling pathway, Rap1 signaling pathway, dopaminergic synapse, adrenergic signaling in cardiomyocytes, oxytocin signaling pathway, cGMP-PKG signaling pathway, and ubiquitin-mediated proteolysis were significantly represented in the KEGG pathway analysis. In addition, our result also showed that mTOR signing pathway plays an important role in the development of TSC-AML and provided more data for clinical use of mTOR inhibitors. Everolimus, a mammalian target of rapamycin (mTOR) inhibitor, has demonstrated its significant reduction in renal angiomyolipoma volume compared with placebo in the phase 3 EXIST-2 trial [30]. Consensus guideline has recommended as the first-line therapy for TSC-AML [31].

In conclusion, this study, to the best of our knowledge, represents the first integrated analysis of miRNA and mRNA expression to explore epigenetic factors in TSC-AML. We identified a number of miRNAs that are differentially expressed in TSC-AML tissues. Furthermore, we reported the altered expression of miRNA processing genes in TSC-AML tissue compared with matched normal adjacent tissue. Renal AML contain an admixture of clonal tumor cells with features of several different mesenchymal lineages, Filipa et al. [7] showed that the renal AML neoplastic stem cells arising from renal epithelial cells. Therefore, it is reasonable for us to use the matched normal renal tissue as the control of TSC-AML. Finally, we constructed a post-transcriptional regulatory network of miRNA-target

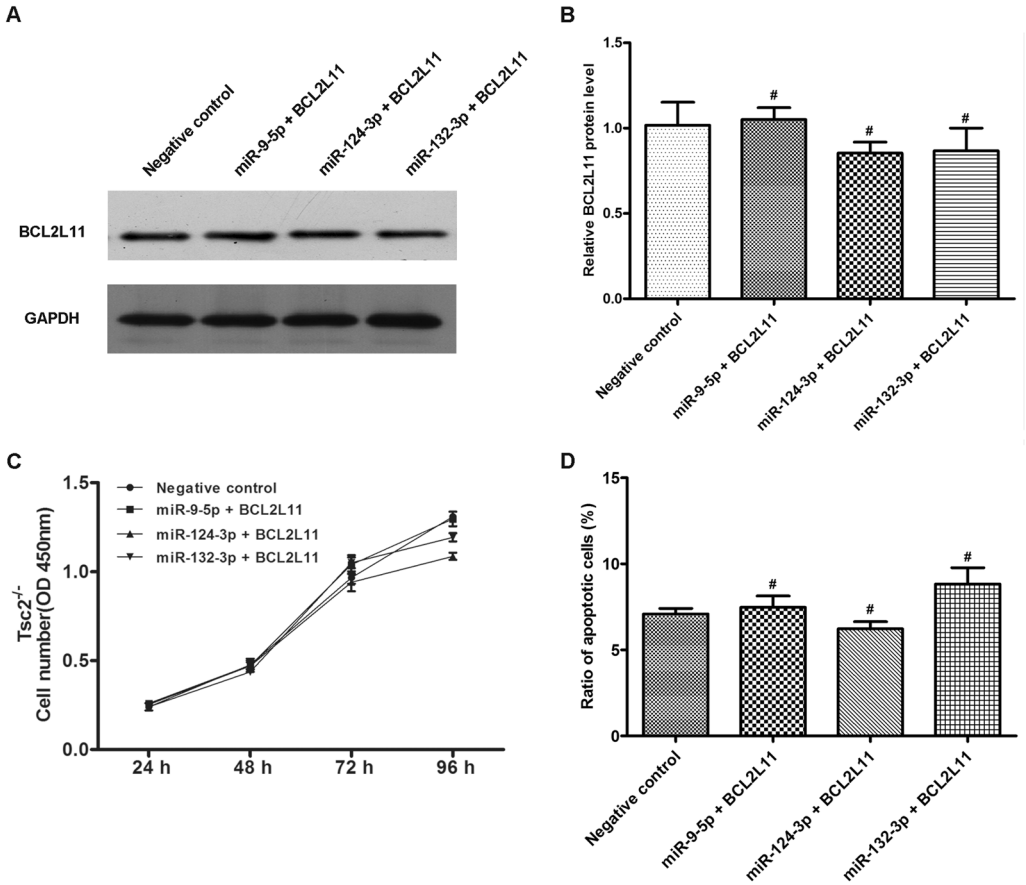

Fig. 7 BCL2L11 rescues the effects of miR-9-5p, miR-124-3p, and miR-132-3p related to the regulation of proliferation and apoptosis in $Tsc2^{-/-}$ cells. **a**, **b** Western blotting analysis of BCL2L11 protein levels in $Tsc2^{-/-}$ cells co-transfected with BCL2L11 lentivirus and miR-9-5p, miR-124-3p, or miR-132-3p mimics or the scrambled control. **a** Representative image. **b** Quantitative analysis. **c** CCK-8 assays were performed 24, 48, 72, and 96 h after the co-transfection of $Tsc2^{-/-}$ cells with BCL2L11 lentivirus and miR-9-5p, miR-124-3p, or miR-132-3p mimics or the scrambled control. **d** $Tsc2^{-/-}$ cells were co-transfected with BCL2L11 lentivirus and miR-9-5p, miR-124-3p, or miR-132-3p mimics or the scrambled control. Apoptosis profiles were analyzed by flow cytometry

gene pairs, identifying BCL2L11 as an endogenous target of miR-9-5p, miR-124-3p, and miR-132-3p in $Tsc2^{-/-}$ cells. Therefore, we propose that miR-9-5p, miR-124-3p, and miR-132-3p, along with their target BCL2L11, may be suitable targets for molecular therapeutic approaches for TSC-AML.

Acknowledgements The research was supported by the National Natural Science Foundation of China (81670611) and the National Key Research and Development Program of China (2016YFC0901500).

Compliance with ethical standards

Conflict of interest The authors declare that they have no conflict of interest.

References

1. Cai Y, Li H, Zhang Y. Assessment of tuberous sclerosis complex associated with renal lesions by targeted next-generation sequencing in mainland China. Urology. 2017;101:170–1.
2. Curatolo P, Bombardieri R, Jozwiak S. Tuberous sclerosis. Lancet. 2008;372:657–68.
3. Northrup H, Krueger DA. Tuberous sclerosis complex diagnostic criteria update: recommendations of the 2012 Iinternational Tuberous Sclerosis Complex Consensus Conference. Pediatr Neurol. 2013;49:243–54.
4. Kapoor A, Girard L, Lattouf JB, Pei Y, Rendon R, Card P, et al. Evolving strategies in the treatment of tuberous sclerosis complex-associated angiomyolipomas (TSC-AML). Urology. 2016;89:19–26.
5. Paradis V, Laurendeau I, Vieillefond A, Blanchet P, Eschwege P, Benoit G, et al. Clonal analysis of renal sporadic angiomyolipomas. Hum Pathol. 1998;29:1063–7.
6. Karbowniczek M, Yu J, Henske EP. Renal angiomyolipomas from patients with sporadic lymphangiomyomatosis contain both neoplastic and non-neoplastic vascular structures. Am J Pathol. 2003;162:491–500.
7. Filipa GA, Adlesic M, Brandt S, Hejhal T, Harlander S, Sommer L, et al. Evidence of renal angiomyolipoma neoplastic stem cells arising from renal epithelial cells. Nat Commun. 2017;8:1466.
8. Ambros V. The functions of animal microRNAs. Nature. 2004;431:350–5.
9. Du T, Zamore PD. Beginning to understand microRNA function. Cell Res. 2007;17:661–3.

10. van Scheppingen J, Iyer AM, Prabowo AS, Muhlebner A, Anink JJ, Scholl T, et al. Expression of microRNAs miR21, miR146a, and miR155 in tuberous sclerosis complex cortical tubers and their regulation in human astrocytes and SEGA-derived cell cultures. Glia. 2016;64:1066–82.
11. Dombkowski AA, Batista CE, Cukovic D, Carruthers NJ, Ranganathan R, Shukla U, et al. Cortical tubers: windows into dysregulation of epilepsy risk and synaptic signaling genes by microRNAs. Cereb Cortex. 2016;26:1059–71.
12. Zhang H, Bajraszewski N, Wu E, Wang H, Moseman AP, Dabora SL, et al. PDGFRs are critical for PI3K/Akt activation and negatively regulated by mTOR. J Clin Invest. 2007;117:730–8.
13. Ma J, Meng Y, Kwiatkowski DJ, Chen X, Peng H, Sun Q, et al. Mammalian target of rapamycin regulates murine and human cell differentiation through STAT3/p63/Jagged/Notch cascade. J Clin Invest. 2010;120:103–14.
14. Concannon CG, Tuffy LP, Weisova P, Bonner HP, Davila D, Bonner C, et al. AMP kinase-mediated activation of the BH3-only protein Bim couples energy depletion to stress-induced apoptosis. J Cell Biol. 2010;189:83–94.
15. Kilbride SM, Farrelly AM, Bonner C, Ward MW, Nyhan KC, Concannon CG, et al. AMP-activated protein kinase mediates apoptosis in response to bioenergetic stress through activation of the pro-apoptotic Bcl-2 homology domain-3-only protein BMF. J Biol Chem. 2010;285:36199–206.
16. Strasser A. The role of BH3-only proteins in the immune system. Nat Rev Immunol. 2005;5:189–200.
17. Kuwana T, Bouchier-Hayes L, Chipuk JE, Bonzon C, Sullivan BA, Green DR, et al. BH3 domains of BH3-only proteins differentially regulate Bax-mediated mitochondrial membrane permeabilization both directly and indirectly. Mol Cell. 2005;17:525–35.
18. Mansha M, Hussain A, Kofler A, Grubbauer C, Goetsch K, Ploner C, et al. "Bam," a novel glucocorticoid-induced BH3-only transcript from the BCL2L11/Bim locus, does not appear to be translated. Leuk Lymphoma. 2013;54:353–8.
19. Frank DO, Dengjel J, Wilfling F, Kozjak-Pavlovic V, Hacker G, Weber A. The pro-apoptotic BH3-only protein Bim interacts with components of the translocase of the outer mitochondrial membrane(TOM). PLoS ONE. 2015;10:e123341.
20. Shukla GC, Singh J, Barik S. MicroRNAs: processing, maturation, target recognition and regulatory functions. Mol Cell Pharmacol. 2011;3:83–92.
21. Coolen M, Katz S, Bally-Cuif L. miR-9: a versatile regulator of neurogenesis. Front Cell Neurosci. 2013;7:220.
22. Leucci E, Zriwil A, Gregersen LH, Jensen KT, Obad S, Bellan C, et al. Inhibition of miR-9 de-represses HuR and DICER1 and impairs Hodgkin lymphoma tumour outgrowth in vivo. Oncogene. 2012;31:5081–9.
23. Wei N, Xiao L, Xue R, Zhang D, Zhou J, Ren H, et al. MicroRNA-9 mediates the cell apoptosis by targeting Bcl2l11 in ischemic stroke. Mol Neurobiol. 2016;53:6809–17.
24. Lee MR, Kim JS, Kim KS. miR-124a is important for migratory cell fate transition during gastrulation of human embryonic stem cells. Stem Cells. 2010;28:1550–9.
25. Cheng LC, Pastrana E, Tavazoie M, Doetsch F. miR-124 regulates adult neurogenesis in the subventricular zone stem cell niche. Nat Neurosci. 2009;12:399–408.
26. Anand S, Majeti BK, Acevedo LM, Murphy EA, Mukthavaram R, Scheppke L, et al. MicroRNA-132-mediated loss of p120RasGAP activates the endothelium to facilitate pathological angiogenesis. Nat Med. 2010;16:909–14.
27. Calin GA, Liu CG, Sevignani C, Ferracin M, Felli N, Dumitru CD, et al. MicroRNA profiling reveals distinct signatures in B cell chronic lymphocytic leukemias. Proc Natl Acad Sci USA. 2004;101:11755–60.
28. Gougelet A, Pissaloux D, Besse A, Perez J, Duc A, Dutour A, et al. Micro-RNA profiles in osteosarcoma as a predictive tool for ifosfamide response. Int J Cancer. 2011;129:680–90.
29. Waardenberg AJ, Basset SD, Bouveret R, Harvey RP. CompGO: an R package for comparing and visualizing gene ontology enrichment differences between DNA binding experiments. BMC Bioinformatics. 2015;16:275.
30. Bissler JJ, Kingswood JC, Radzikowska E, Zonnenberg BA, Frost M, Belousova E, et al. Everolimus for angiomyolipoma associated with tuberous sclerosis complex or sporadic lymphangioleiomyomatosis (EXIST-2): a multicentre, randomised, double-blind, placebo-controlled trial. Lancet. 2013;381:817–24.
31. Krueger DA, Northrup H. Tuberous sclerosis complex surveillance and management: recommendations of the 2012 International Tuberous Sclerosis Complex Consensus Conference. Pediatr Neurol. 2013;49:255–65.